Dixon Chemical Species Separation

Michael A. Mendoza, Stephen J. Preston

***Abstract*— Chemical species separation methods utilize phase information to separate chemical species in Magnetic Resonance images to improve medical diagnosis. The origin of this phase information is discussed along with various algorithmic implementations which use this phase information for chemical species separation. Particular attention is paid to the implementation of the IDEAL algorithm.**

***Index Terms*—Dixon Chemical Species Separation, Iterative Decomposition with Echo Asymmetry and Least-Squares Estimation, IDEAL**

I. Introduction

Most of the body is comprised of water, which is the prime source of signal and dynamic contrast in MRI images of human tissues. However, fat is also ubiquitous throughout the body and often surrounds and obscures tissues and pathologies of interest in MRI images. In order to improve fat obscured images, fat suppression or chemical species separation techniques are used.

Fat suppression in MRI imagery has a number of benefits. With fat suppression, MRI image dynamic contrast can be improved for less abundant, but potentially interesting tissues/metabolites such as the musculoskeletal system and articular cartilage. In addition to improving dynamic contrast, fat suppression is useful for improving variety of medical diagnoses. For example, fat suppression is useful for preventing costly incorrect cancer diagnoses which can occur when fat infiltrates cellular cytoplasm and is mistaken as a metastatic tumor in traditional MRI. Finally, chemical species separation is important for the correction tissue location errors in MRI images that arise because of the perturbation that the chemical shift cause in MRI spatial encoding.

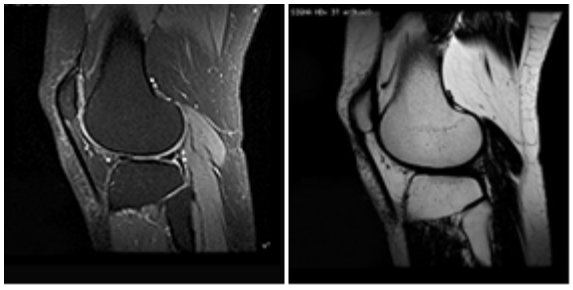

Figure 1: Water (left) and Fat (right) MRI images after Chemical Species Separation (Courtesy of General Electric).

II. Theory

Dixon Chemical Species Separation is an important MRI technique for fat suppression in MRI imagery. This technique suppresses the fat in MRI imagery by partitioning the original image into two separate water and fat images as shown in Figure 1. This process is possible because different chemicals substances resonate at different frequencies when using MRI techniques.

In MRI, the tissue to be imaged is placed in a strong magnetic field, $\mathbf{B_0}$. This field causes the magnetic moments of the hydrogen nuclei in the tissue to align with the magnetic field. This forms a net magnetization vector in the direction of $\mathbf{B_0}$. The transverse component (or the component orthogonal to the $\mathbf{B_0}$ axis) of the net magnetization vector generates the signal which is transformed into MRI images. This signal is generated when the net magnetization vector is then tipped away from the $\mathbf{B_0}$ axis, by exciting the nuclei with RF energy. Consequentially this will cause the magnetic moments to precess about the $\mathbf{B_0}$ axis in the transverse plane at a frequency called the Larmor frequency.

The Larmor frequency is proportional to the strength of the magnetic field felt by the hydrogen nuclei. Therefore a change in the effective $\mathbf{B_0}$ felt by these nuclei causes a change in the precession rate of the net magnetization vector about $\mathbf{B_0}$. In various molecular substances the hydrogen nuclei are shielded by adjacent atoms from the full strength of $\mathbf{B_0}$. When compared to lone hydrogen nuclei, this causes a shift in their precession rate known as the chemical shift.

Important for chemical species separation techniques is the idea that due to the chemical shift, the protons of different chemical substances resonate at a different. For water and fat this difference in the chemical shift is about 3.5 parts per million which for a 3 T magnet corresponds to about a 430 Hz difference in their Larmor frequencies.

This difference in their Larmor frequencies causes a time-varying phase difference in water and fat signals in MRI images. Since fat and water precess at different relative frequencies, images taken at different times will carry different relative phase shifts for water and fat NMR signals. By utilizing images with different relative phase shifts, the signal associated with each resonant frequency can be selected. This allows for the separation of fat, and water, as well as other chemical species across multiple MRI images.

III. Algorithms

Three different Dixon Chemical Species Separation algorithms will be outlined, including: 1) 'Two-point Dixon,' 2) 'Three-point Dixon,' and 3) '*Iterative Decomposition with Echo Asymmetry and Least Squares Estimation* (IDEAL)'. These algorithms are listed in order of complexity, with each subsequent algorithm offering improved image SNR, improved chemical species separation as well as other additional capabilities.

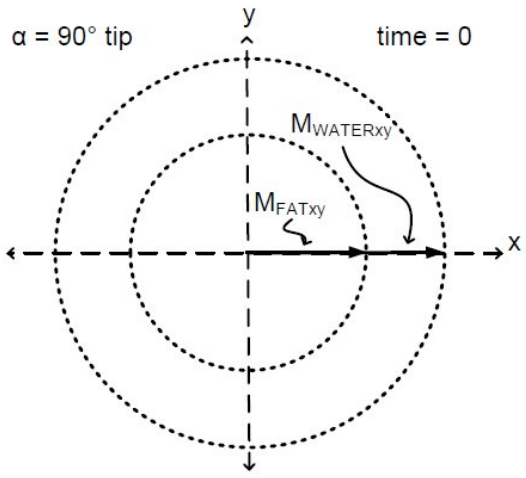

Figure 2: Graphical representation of water and fat magnetization vectors in-phase

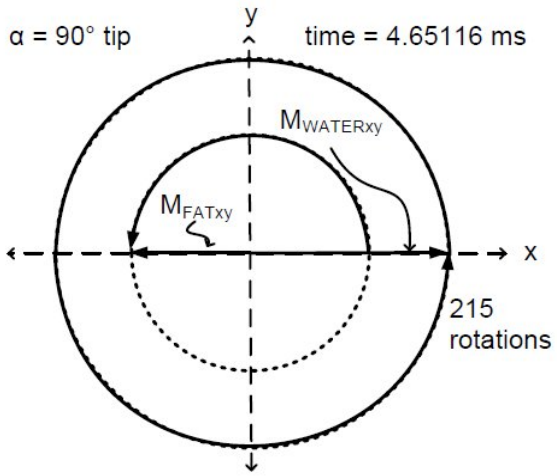

Figure 3: Graphical representation of water and fat magnetization vectors out-of--phase

A. Two-Point Dixon

The Two-Point Dixon Image Reconstruction algorithm is the original Dixon Chemical Species algorithm, introduced in 1984, and it receives its name from both its inventor and the fact that it requires two distinct MRI images to separate fat from water. Although simplest separation method, it is useful because it does provide a nice starting point for developing a basic understanding and intuition on how multiple images can be used to separate chemical species.

The Two-Point Dixon algorithm depends on combining two MRI images with select phase relationships in order to separate water from fat. In the first image, the signal must be sampled when the transverse magnetization vector for fat and water are in phase with each other, as shown in Fig 1. In the 2nd image, the MRI data must be sampled when the transverse magnetization vectors are out of phase with each other, which corresponds to a phase difference of 180 degrees, as shown in Fig. 2.

The actual algorithm is quite simple. Once the data the data from the two images is acquired, in order to produce a water image the images are simply added together and in order to produce a fat image they are subtracted from each other.

The water image is formed by addition because across the two images the fat signal is 180 degrees out of phase. This causes the cancelation of the fat signal when the two images are added together. In contrast, when the two images are subtracted from each other, the water signal is effectively 180 degrees out of phase, and a fat image is formed.

Images were generated to demonstrate the effectiveness of this algorithm as shown in Figure 4. The original image was taken from an anonymous breast sample. They were generated from an in-phase and an out-of-phase data set. As can be clearly seen, the water and fat components of the signal were successfully separated using this technique.

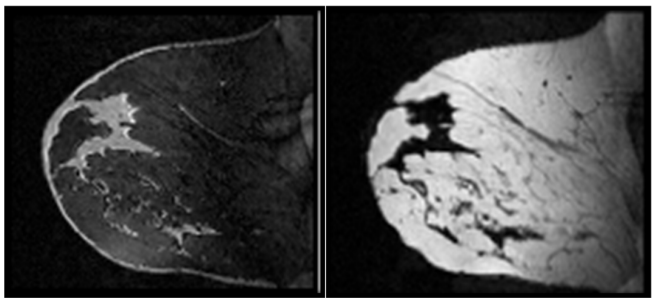

Figure 4: Water (left) and Fat (right) MRI images after Two-Point Chemical Species Separation

B. Three-Point Dixon

Ideally the strong magnetic field, $\mathbf{B_0}$, used in MRI would be spatial consistent and homogenous in intensity across the sample to be imaged. Unfortunately, this is not true and the inhomogenities in the magnetic field felt by the hydrogen nuclei cause phase errors in MRI images which can make chemical separation difficult. Improved chemical species separation algorithms, therefore, must account for these field inhomogeneities. This is what the Three-Point Dixon and the IDEAL algorithm attempt to do.

The Three-Point Dixon algorithm attempts to account for these field inhomogeneities by using a third image in order to create a field map, which is mapping of phase inhomogeneities across the image. The signal for third image is sampled when the water and fat signals are back in phase, which corresponds to a 2π phase difference between the first and third images.

Since the water and fat signals are in phase, it possible to extract the phase differences or inhomogenities in the phase across the sample by the relation in Eq. [1].

$$\phi = \frac{\angle m_1 m_3^*}{2} \quad [1]$$

While, not a perfect estimate of the map field, this technique is a useful first order approximation of the field inhomogeneities in MRI images. Figure 5 shows the field map for the anonymous breast sample data used in earlier. This data will be used for improved chemical species separation according in the Three-Point Dixon algorithm.

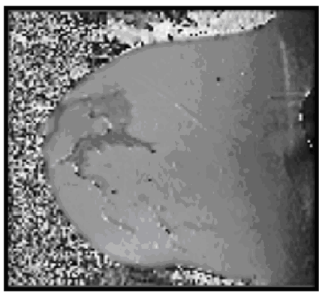

Figure 5: Field map of field heterogeneities for use in Three-Point Dixon Algorithm

Once an estimate of the field map is created, the field map can be used as indicated in Equations [2] and [3], which are used to generate water and fat images.

$$m_{water} = \frac{1}{2}\left(m_1 + m_2 e^{-i\varphi}\right) \quad [2]$$

$$m_{fat} = \frac{1}{2}\left(m_1 - m_2 e^{-i\varphi}\right) \quad [3]$$

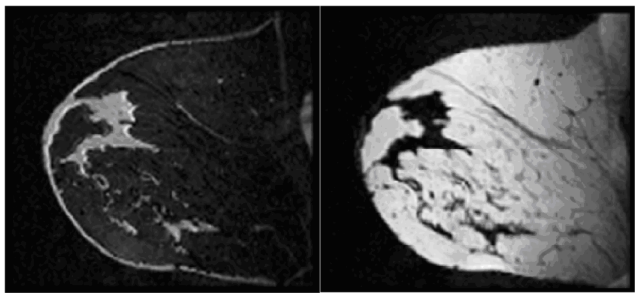

Figure 6: Water (left) and Fat (right) MRI images after Two-Point Chemical Species Separation

Images were generated to demonstrate the effectiveness of the Three-Point Dixon algorithm as shown in Figure 6. Comparison of results of the Two-Point and the Three-Point Dixon implementations show little difference between the images. Normally this is not true, because of field inhomogenities. However, with this data set the field map was found to be rather homogenous so that field inhomogenities had a negligible effect on the decomposed water and fat images. In order to better visualize the improvements between the two Dixon Reconstruction methods, the difference of the magnitudes of the water images was generated in Figure 7. As can be seen, the Three-Point Dixon algorithm resulted in a slight improvement in the decomposed image SNR.

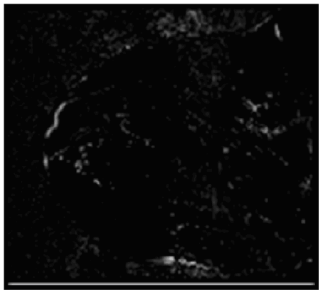

Figure 7: Comparison of Two-Point and Three-Point Dixon Algorithms (Differences of signal magnitudes for water images multiplied by a factor of 4)

C. Iterative Decomposition with Echo Asymmetry and Least Squares Estimation (IDEAL)

Chemical species separation is an important MRI technique for medical diagnosis. The problem with some chemical separation methods, like the simple Dixon Reconstruction algorithms outlined earlier, is that they suffer from sub-optimal SNR and/or the inability to reliably create separate chemical images of all body tissues. IDEAL is more advanced chemical separation technique which attempts to address theses issues. In addition, IDEAL is also a superior technique because it allows for fast image acquisition, as well as the simultaneous separation of chemical species.

IDEAL solves these issues by using an iterative least squares estimation method in order to solve the nonlinear estimation of the field map of an MRI image. Ultimately, this field map estimate is superior to the estimate of the 3-point Dixon algorithm because the nonlinear least squares estimation technique corresponds to the optimal maximum likelihood estimate in the presence of Gaussian noise. With this field map estimate, IDEAL is able to create a superior decomposition of chemical species from the original MRI image.

1) Iterative Least-Squares Estimation Method

The MRI signal of each pixel can modeled (as shown in Eq. [4]) as being the sum of the signal components of each chemical species (ρ_j) multiplied by phase terms corresponding to the phase of the signal at the time (t_n) of sampling for each chemical species with a chemical shift (Δf_j) and to the phase due to the perturbation of the signal from field heterogeneities which are represented in the field map, ψ.

TABLE I
SUMMARY OF COST/BENEFITS OF VARIOUS CHEMICAL SPECIES SEPARATION ALGORITHMS

Algorithm	Benefits	Cost
Two-Point Dixon	• Simplest Implementation	• Poorest Image SNR • Inaccurate Image Separation when Field Heterogeneities Present
Three-Point Dixon	• Simple Implementation • Improved Image SNR	• Requires a Field Map Estimate
IDEAL	• Fast Image Acquisition Capable • Improved Image SNR • Multiple Chemical Species Separation	• Algorithm Complexity • Computationally Expensive

$$s_n = \left(\sum_{j=1}^{N} \rho_j e^{i2\pi\Delta f_j t_n} \right) e^{i2\pi\psi t_n} \quad [4]$$

One of the nice of characteristics of this signal representation is that IDEAL algorithm is designed to separate of up to M chemical substances with various chemical shifts as long as M+1 images of MRI data are available. However, the problem with Eq. [4] is that perturbation of the signal due to the field map makes it a nonlinear estimation problem. This makes it difficult to estimate signal components of the individual chemical species without knowing the field map beforehand. So in order to order to separate chemical species, an accurate estimate of the field map is needed.

$$\hat{s}_n = s_n e^{-i2\pi\psi_0 t_n} = \sum_{j=1}^{N} \rho_j e^{i2\pi\Delta f_j t_n} = A\rho \quad [5]$$

$$\rho = (A^T A)^{-1} A^T \hat{S} \quad [6]$$

Assuming an estimate of the field map is known then the previous relation (Eq. [4]) then it can be rewritten in matrix form as a linear set of equations unperturbed by field heterogeneities (Eq. [5]) from which an ordinary least squares (OLS) estimation can be made to estimate the individual signal components as shown in Eq. [6] [1]

In order to estimate the field map, initial estimates the signal from each chemical species (ρ_j) are made from Eq.[6] using an initial guess of zero Hz for the field map, ψ. Using this initialize estimate of ρ_j, the following iterative least squares algorithm is used estimate the field map:

1. The field map error, $\Delta\psi$, is calculated using a linearized signal equation and OLS.
2. The field map is recalculated: $\psi = \psi_0 + \Delta\psi$.
3. The unperturbed signal is recalculate using Eq.[5] with the new estimate of ψ.
4. Steps 2-4 are repeated until error in the field map is small (e.g. $\Delta\psi < 1$ Hz)

The estimation of the field map error, $\Delta\psi$, is made by assuming that there exists some error in the signal components of the chemical species and in the field map. Assuming this, ρ_j and ψ can be rewritten as in Eq. [7]. These variables represent the quantities to be estimated in the subsequent OLS estimation to be made on signal equation after it is linearized.

$$\rho_j \approx p_{j0} + \Delta\rho_j \quad \psi \approx \psi_0 + \Delta\psi \quad [7]$$

Using these new relations for ρ_j and ψ, it can be shown that Eq. [4] can be rewritten as Eq. [8]. And consequently, a new set of equations for the MRI signal unperturbed by field heterogeneities can be shown to be written as Eq. [9].

$$s_n = \left(\sum_{j=1}^{N} (\rho_j + \Delta\rho_j) e^{i2\pi\Delta f_j t_n} \right) e^{-i2\pi(\psi_0 + \Delta\psi)t_n} \quad [8]$$

$$\hat{s}_n = \left(\sum_{j=1}^{N} (\rho_j + \Delta\rho_j) e^{i2\pi\Delta f_j t_n} \right) e^{-i2\pi\Delta\psi t_n} \quad [9]$$

Finally in order to calculate an estimate of the field map error using OLS, Eq. [9] is linearized by taking a Taylor expansion of the phase term shown in Eq. [10].

$$e^{-i2\pi\Delta\psi t_n} \approx 1 + i2\pi\Delta\psi t_n \quad [10]$$

Using this Taylor expansion, the unperturbed signal equation can be written as a linearized set of equations as in Eq. [11] which can be written in matrix form as shown in Eq. [12].[2]

[1] A matrix used in calculations can be found in Appendix A in [2].

[2] B matrix used in calculations can be found in Appendix A in [2].

$$\hat{\hat{s}}_n = \left(\sum_{j=1}^{N} (\rho_j + \Delta\rho_j) e^{i2\pi\Delta f_j t_n} \right) (1 + i2\pi\Delta\psi t_n) \quad [11]$$

$$\hat{\hat{s}}_n = By \quad [12]$$

Then using a linear least squares estimation, the errors in ρ and ψ can be calculated as shown in Eq. [13].

$$y = (B^T B)^{-1} B^T \hat{\hat{S}} \quad [13]$$

$$y = \begin{bmatrix} \Delta\psi & \Delta\rho & \Delta\rho & \dots & \Delta\rho & \Delta\rho \end{bmatrix} \quad [14]$$

From these calculations, the quantity of interest, $\Delta\psi$, can be extracted from the vector y. With this $\Delta\psi$, ψ is recalculated ($\psi = \psi_0 + \Delta\psi$) and then Eq. [5] is recalculated. This iterative procedure is repeated using the new values for the field map until the error converges to a desired threshold (e.g. $\Delta\psi < 1$ Hz).

This outlined procedure is done for each and every pixel in the MRI images, and then after an accurate field map is created for the MRI image, a low-pass filter is used to spatially smooth the final map. With this final field map estimate, OLS is used again to create a final estimate of the chemical species components in the MRI images using Equation [6].

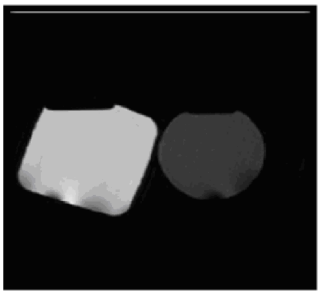

Figure 8: Water (left) and Fat (right) test image for IDEAL

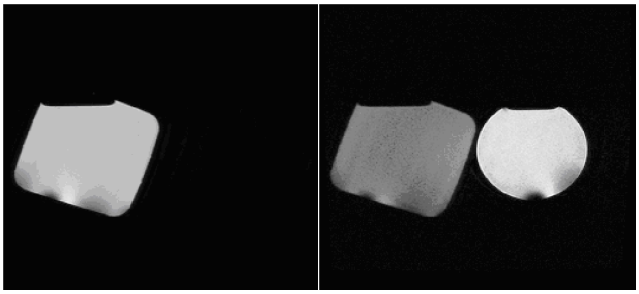

Figure 9: Water (left) and Fat (right) MRI images after current IDEAL algorithm implementation

2) Algorithm Implementation Results

The IDEAL algorithm was implemented in an attempt to demonstrate the effectiveness of the algorithm when compared to the Two-Point and Three-Point Dixon Reconstruction algorithms. Unfortunately, due to the difficultly of implementing the algorithm and time-constraints a fully functioning algorithm was not implemented.

Using the current form of the MATLAB code on the MRI image data set shown in Figure 8 water and fat were partial separated. Figure 9 demonstrates the effectiveness of this separation. As can be seen, water was completely isolated in the left image, however fat was not completely isolated in the right one. Future work will be done to fix any bugs in the implementation of the IDEAL code to allow for complete chemical species separation.

IV. Conclusions

Dixon Chemical Species Separation is an important MRI technique for fat suppression in MRI imagery. This technique allows for fat suppression in MRI imagery by partitioning the original image into two separate water and fat images which is useful for improved image dynamic contrast and improved medical diagnosis. Three Chemical Species Separation algorithms were explored and implemented. The three-Point Dixon Reconstruction was found to be a superior chemical separation technique when compared to Two-Point Dixon algorithm. Among the all three of the algorithms implemented IDEAL was thought to be the most superior decomposition technique because of its ability to create the most accurate estimate of the field map for chemical decomposition, however due to it's complexity and time constraints this technique was not successfully implemented.

References

[1] W.T.Dixon, Simple Proton Spectroscopic Imaging, *Radiology*, 152:189-194, 1984

[2] S.B. Reader, Z., Wen, H. Yu, A.R. Pineda, G.E. Gold, M. Markl, and N.J. Pelc, Multicoil Dixon Chemical Species Separation with an Iterative Least-squares Estimation Method, *Magnetic Resonance in Medicine* 51:35-45, 2004.

[3] J. Pauly, Field Maps, *Stanford Lecture*, October 8, 2007.

[4] J. Pauly, Field Maps, *Stanford Lecture*, October 8, 2007.

APPENDIX: PROJECT MATLAB CODE

```
% ECEn 682R Project
% Michael Mendoza
% Stephen Preston

clear;
%%
% 2 Point Dixon Reconstruction
if(0)

% m=load('.\Stephen\IMS_606_607.mat');
% m1=m.im1; m2=m.im2;
% m=load('.\Stephen\IMS_632_633.mat');
% m1=squeeze(m.im1(100,:,:)); m2=squeeze(m.im2(100,:,:));

m1amp=dicomread('.\Breast_Anonymous\gm_gre te 4.7 - 10\IM-0001-0100.dcm');
m1phase=dicomread('.\Breast_Anonymous\gm_gre te 4.7 - 11\IM-0001-0100.dcm');
m1amp=cast(m1amp,'single'); m1phase=cast(m1phase,'single');
m1phase=(m1phase/4095)*2*pi;
m1=m1amp.*exp(i*m1phase);

m2amp=dicomread('.\Breast_Anonymous\gm_gre te 5.75 - 8\IM-0001-0100.dcm');
m2phase=dicomread('.\Breast_Anonymous\gm_gre te 5.75 - 9\IM-0001-0100.dcm');
m2amp=cast(m2amp,'single'); m2phase=cast(m2phase,'single');
m2phase=(m2phase/4095)*2*pi;
m2=m2amp.*exp(i*m2phase);

mw=0.5*(m1+m2);
mf=0.5*(m1-m2);

figure(1);
%imshow(abs(mw)',[0 0.07])
imshow(abs(mw)',[0 460])
figure(2);
%imshow(abs(mf)',[0 0.07])
imshow(abs(mf)',[0 660])

end
%%
% 3 Point Dixon Reconstruction
if(0)

m1amp=dicomread('.\Breast_Anonymous\gm_gre te 4.7 - 10\IM-0001-0100.dcm');
m1phase=dicomread('.\Breast_Anonymous\gm_gre te 4.7 - 11\IM-0001-0100.dcm');
m1amp=cast(m1amp,'single'); m1phase=cast(m1phase,'single');
m1phase=(m1phase/4095)*2*pi;
m1=m1amp.*exp(i*m1phase);

m2amp=dicomread('.\Breast_Anonymous\gm_gre te 5.75 - 8\IM-0001-0100.dcm');
m2phase=dicomread('.\Breast_Anonymous\gm_gre te 5.75 - 9\IM-0001-0100.dcm');
m2amp=cast(m2amp,'single'); m2phase=cast(m2phase,'single');
m2phase=(m2phase/4095)*2*pi;
m2=m2amp.*exp(i*m2phase);

m3amp=dicomread('.\Breast_Anonymous\gm_gre te 6.8 - 6\IM-0001-0100.dcm');
m3phase=dicomread('.\Breast_Anonymous\gm_gre te 6.8 - 7\IM-0001-0100.dcm');
m3amp=cast(m3amp,'single'); m3phase=cast(m3phase,'single');
m3phase=(m3phase/4095)*2*pi;
m3=m3amp.*exp(i*m3phase);
```

```
phi=angle(conj(m1).*m3)/2;

mw3=0.5*(m1+m2.*exp(-i*phi));
mf3=0.5*(m1-m2.*exp(-i*phi));

figure(3);
imshow(abs(mw3)',[0 460]);
figure(4);
imshow(abs(mf3)',[0 660]);

end

%% Comparsion
if(0)
    figure(5);
    imshow(abs(mw3)'-abs(mw)',[0 460/10]);
    figure(6);
    imshow(abs(mf3)'-abs(mf)',[0 660/10]);
end

%%
% IDEAL

if(1)
Threshold=0.5;
dF=[0 430];
%dF=[0 -220];

% Load Data
load idealexample.mat;
t=[-0.0004 0.0011 0.0027];
%t =  [-0.000378787878788 0.001136363636364 0.002651515151515];
%t=[0.0004 0.0011 0.0027];
m1=IM1; m2=IM2; m3=IM3;
N = 3; M = 2;  %Number of Images/ Number of Species
im(1,:,:)=m1;
im(2,:,:)=m2;
im(3,:,:)=m3;
% load IMS_606_607.mat;
%
% imshow(IMS_606_607,[])

% Load S vector
J=length(m1(:,1));
K=length(m1(1,:));
Sdata=zeros(2*N,J,K);
S_dhat=zeros(6,1);
gR=zeros(1,N);
gI=zeros(1,N);
B=zeros(2*N,5);
dpR=zeros(1,M);
dpI=zeros(1,M);
%p =zeros(6,1);
pimage1=zeros(J,K);
pimage2=zeros(J,K);
for n=1:N
    for j=1:J
        for k=1:K
            Sdata(n,j,k)  =real( im(n,j,k) );
            Sdata(N+n,j,k)=imag( im(n,j,k));
        end
    end
end
```

```
% Fill c and d
for j=1:M % Species
   for k=1:N % Images
      c(j,k)=cos(2*pi*dF(j)*t(k));
      d(j,k)=sin(2*pi*dF(j)*t(k));
   end
end

% Fill A
j=2; % Using special case for A in Appendix C
A=zeros(2*N,4);
for k=1:N
    A(k,:)    =[1, 0, c(j,k), -d(j,k)];
    A(N+k,:)  =[0, 1, d(j,k), c(j,k) ];
end

% Loop through for each pixel
for px=1:K
%for px=110:140
    for py=1:J

        %Load Data
        S_hat=Sdata(:,px,py);

        % Estimate singal of each species
        p = (A.'*A)\(A.'*S_hat);

        % Set Flags and Counters
        wflag=1;
        count=0;

        % Check if pixel is zero
        if(Sdata(1,px,py)==0 && Sdata(2,px,py)==0)
           wflag=0;
        end

        %%%%%%%%%%%%%%%%%%%%%%%%%%%%%%%%%%%%%%%%%%%%%%%%%%%%%%%%%%%%%%%%%%%%%%%%%%%
        % Loop through while psi error is > threshold
        dPsi = 2*Threshold;
        psi0 = 0;
        while(dPsi>Threshold && wflag==1)

            % Fill B
            j=2; % Using special case for B in Appendix C
            for k=1:N
                gR(k)=2*pi*t(k)*(-p(2)-p(3)*d(j,k)-p(4)*c(j,k));
                gI(k)=2*pi*t(k)*(p(1)+p(3)*c(j,k)-p(4)*d(j,k));
                B(k,:)    =[gR(k), 1, 0, c(j,k), -d(j,k)];
                B(N+k,:)  =[gI(k), 0, 1, d(j,k), c(j,k) ];
            end

            % Estimate of error
            % Calc S_dhat
            for n=1:N
                temp0=0;
                temp1=0;
                for j=1:M
                    idR=2*(j-1)+1;
                    idI=2*(j-1)+2;
                    temp0=temp0+(p(idR)*c(j,n)-p(idI)*d(j,n));
                    temp1=temp1+(p(idR)*d(j,n)+p(idI)*c(j,n));
                end
```

```
                S_dhat(n)  =S_hat(n)-temp0;
                S_dhat(N+n)=S_hat(N+n)-temp1;
            end


            [px,py]
            % Calculate Error Estimates
            y=(B.'*B)\(B.'*S_dhat);

            dPsi=y(1);
            for j=1:M
                dpR(j)=y(2*j);
                dpI(j)=y(2*j+1);
            end

            % Recalculate Psi
            psi0=psi0+dPsi;

            % Recalculate S_hat
            for n=1:N
                Stemp=(Sdata(n,px,py)+i*Sdata(n+N,px,py))*exp(-i*2*pi*psi0*t(n));
                S_hat(n)  =real(Stemp);
                S_hat(n+N)=imag(Stemp);
            end

            count=count+1
            psivec(count) = psi0;
            dPsivec(count)= dPsi;
        end

        % Save Fat and Water Consentrations
        if(wflag==1)
            pimage1(px,py)=sqrt(p(1)*p(1)+p(2)*p(2));
            pimage2(px,py)=sqrt(p(3)*p(3)+p(4)*p(4));
        else
            pimage1(px,py)=0;
            pimage2(px,py)=0;
        end
    end
end

figure(1);
imshow(pimage1(:,:),[]);
figure(2);
imshow(pimage2(:,:),[]);
figure(3);
imshow(abs(m1),[]);
end
```
